Mind the translational gap: human microglia differ from mouse microglia in their regulation of K_v and $K_{ir}2.1$ channels

Simone Schilling[1,2,3,4], Jessica Felk[1], Majed Kikhia[1,2,5], Alice Podestà[1,8], Johanna Hintze[1], Pawel Fidzinski[1,7,8], Martin Holtkamp[1,6,7], Julia Onken[9], Thomas Sauvigny[10], Thilo Kalbhenn[11], Matthias Simon[11], Helmut Kettenmann[12, 13], Matthias Endres[1,2,3,5], Ria Göttert[#,1,2,3] & Karen Gertz[*,#,1,2,3,5]

1. Charité – Universitätsmedizin Berlin, Corporate Member of Freie Universität Berlin and Humboldt-Universität zu Berlin, Department of Neurology and Experimental Neurology, Charitéplatz 1, 10117 Berlin, Germany
2. Charité – Universitätsmedizin Berlin, Corporate Member of Freie Universität Berlin and Humboldt-Universität zu Berlin, Center for Stroke Research Berlin (CSB), Charitéplatz 1, 10117 Berlin, Germany
3. German Centre for Cardiovascular Research (DZHK), Partner Site Berlin, Berlin, Germany
4. Berlin Institute of Health at Charité - Universitätsmedizin Berlin, Charitéplatz 1, 10117 Berlin, Germany
5. Charité – Universitätsmedizin Berlin, Corporate Member of Freie Universität Berlin and Humboldt-Universität zu Berlin, Einstein Center for Neurosciences Berlin, Charitéplatz 1, 10117 Berlin, Germany.

6. Epilepsy-Center Berlin-Brandenburg, Ev. Krankhaus Königin Elisabeth Herzberge, Herzbergstr. 79, 10365 Berlin, Germany
7. Charité – Universitätsmedizin Berlin, Corporate Member of Freie Universität Berlin and Humboldt-Universität zu Berlin, Department of Clinical and Experimental Epileptology, Charitéplatz 1, 10117 Berlin, Germany
8. Charité – Universitätsmedizin Berlin, Corporate Member of Freie Universität Berlin and Humboldt-Universität zu Berlin, Institute of Neurophysiology, Charitéplatz 1, 10117 Berlin, Germany
9. Charité – Universitätsmedizin Berlin, Corporate Member of Freie Universität Berlin and Humboldt-Universität zu Berlin, Department of Neurosurgery, Charitéplatz 1, 10117 Berlin, Germany
10. Department of Neurosurgery, University Medical Center Hamburg-Eppendorf, Hamburg, Germany
11. Department of Neurosurgery, Evangelisches Klinikum Bethel, Universitätsklinikum Ostwestfalen-Lippe, Bielefeld, Germany
12. Max-Delbrück-Center (MDC) for Molecular Medicine in the Helmholtz Association, Berlin-Buch, Germany.
13. Shenzhen University of Advanced Technology, Shenzhen, China.

[#] denotes equal contribution

* Correspondence should be addressed to Prof. Dr. Karen Gertz, Department of Neurology and Experimental Neurology, Charité - Universitätsmedizin Berlin, Charitéplatz 1, 10117 Berlin, Germany; Email: karen.gertz@charite.de

Abstract

K^+ channels are important for controlling membrane potential and regulating functional properties of microglia. Whereas the inward-rectifying K^+ (K_{ir}) channel 2.1 modulates proliferation, voltage-gated K^+ channels (K_v) are linked to inflammatory response in mouse microglia (mMG). These channels serve as possible drug targets but little is known regarding their activity in human microglia.

We used patch-clamp recording to study membrane currents of primary human microglia (hMG) and human induced pluripotent stem cell-derived microglia-like cells (hiPSC-MGL) and compared them with mMG. Unlike mMG, hMG and hiPSC-MGL exhibited $K_{ir}2.1$ currents only after LPS+IFN-γ stimulation. Interestingly, K_v currents were not observed in hMG or hiPSC-MGL under any condition. While mMG had a progressively ameboid morphology after stimulation, hMG showed few morphological changes and hiPSC-MGL increased ramification.

Overall, the activity of $K_{ir}2.1$ and K_v channels in hMG and hiPSC-MGL differs fundamentally from mMG. Our findings highlight differences between species and underscore the need for translational approaches.

Introduction

Microglia are the resident immune cells of the central nervous system (CNS) and play essential roles in maintaining homeostasis, responding to injury, and regulating neuroinflammation [1]. In their surveillant state, microglia exhibit a highly ramified morphology, continuously monitoring the brain microenvironment *in vivo*. Upon activation, they undergo rapid morphological changes, transitioning to an amoeboid shape characterized by retracted processes and enlarged soma - a phenomenon well-characterized in rodent models [2-4]. This morphological shift is accompanied by functional changes, including the release of cytokines and chemokines such as TNF-α, IL-6, IL-1β, and CCL2 [5]. These secretion patterns are well established in rodent microglia and increasingly reported in human microglial models [6].

Furthermore, microglia express a range of ion channels, which are essential for maintaining membrane potential and regulating context-dependent responses [7]. Patch-clamp electrophysiology allows high-temporal resolution of microglial ion channel activity, under resting and activated conditions, offering insights into microglial responses to pathological stimuli [8]. Rodent microglia have been characterized using patch-clamp recordings under various conditions. *In vivo,* mouse microglia express low levels of K^+ channels, however, after a pathological challenge, inward-rectifying K^+ channels are upregulated first [4, 8]. Cultured mouse microglia (mMG) constitutively express these inward-rectifying K^+ channel. Upon stimulation, e.g. by facial axotomy, stab wound or in the context of stroke, mouse microglia express outward-rectifying, voltage-gated K^+ channels [4, 9, 10].

$K_{ir}2.1$ (*KCNJ2* gene) is the predominant inward-rectifying K^+ channel in microglia and contributes to the maintenance of the resting membrane potential, thereby regulating activation and responsiveness. It plays a key role in stabilizing microglial homeostasis and modulating their response to inflammation [11]. Microglia also express several outward-rectifying, voltage-gated K^+ channels of the K_v family, with $K_v1.3$ being the most extensively studied [12-

14]. $K_v1.3$ is a voltage-gated K^+ channel that contributes to membrane repolarization and calcium influx required for functions such as cytokine release, proliferation, and migration [13]. $K_v1.3$ is upregulated in activated mouse microglia *in vivo* and *in vitro*, highlighting its relevance in neuroinflammatory and neurodegenerative conditions [12, 14]. It has therefore been suggested as a potential drug target to alter microglia activity [15]. Although the presence of $K_v1.3$ has been reported in human microglia in histology and sequencing data, there is a lack of data demonstrating its functional relevance in human microglia [16].

Translation of microglial findings from mouse models to clinical applications has been challenging, in part due to limited access to human cells and tissue. Primary human microglia in culture (hMG) are a precious resource, as surgical tissue is not widely available and often represents pathological conditions. We have previously studied hMG to investigate the properties of human microglia [17]. In addition, human induced pluripotent stem cell-derived microglia-like cells (hiPSC-MGL) represent an increasingly used alternative model that may better reflect human microglial physiology while reducing reliance on animal experiments [17, 18]. However, their application depends on thorough characterization, and electrophysiological data remains scarce.

In this study, we investigated the properties of hMG and hiPSC-MGL in comparison to the well-established mMG, focusing in particular on electrophysiological functions and the activity of potassium channels. Our work underscores the importance of translational approaches.

Material and Methods

Primary mouse microglia (mMG)

All experimental procedures were approved by the respective official committees and carried out in strict accordance with the Animal Welfare Act and the ARRIVE (Animals in Research: Reporting In Vivo Experiments) guidelines.

Primary mouse microglia (mMG) were isolated from C57BL/6J wildtype male and female mice at postnatal day 3 using a previously published and well-established protocol [19]. In summary, mMG were collected using a gentle shake-off method. The cells were left in culture for an additional 24 hours before use. All experiments were conducted in DMEM supplemented with 10% fetal calf serum, 1% Pen/Strep, 1% sodium pyruvate, and 4.5 g/l d-glucose ("complete medium").

Primary human microglia (hMG)

Primary human microglia (hMG) were isolated from surgery tissue of patients with medication-resistant epilepsy after prior written consent. The ethics committee of the Charité Universitätsmedizin Berlin (EA2/111/14) approved all procedures. The age and sex of the patients included in this study are given in Suppl. Table 1. The microglia were isolated according to previously published protocols with slight modifications [20]. In summary, blood vessels and meninges were carefully removed from resected brain tissue using a dissection microscope (Zeiss Stemi DV4, Oberkochen, Germany). The tissue was then weighed, diced, and dissociated with the Neural Tissue Dissociation Kit (P) (#130–092-628, Miltenyi Biotec, Bergisch Gladbach, Germany). The resulting microglia were cultured as adherent cells in poly-L-lysine coated T75 flasks with microglia culture medium, which included DMEM/F12, 10% fetal calf serum, and 1X penicillin–streptomycin solution. After 1 week of incubation at 37°C and 5% CO2, cells were transferred to multiwell plates for further experiments. To detach the

cells, the culture medium was removed, and the flasks were washed with phosphate-buffered saline (PBS, without Mg++ and Ca++). Cells were then incubated with 3 ml Trypsin/EDTA solution (0.25%/0.02%) at 37°C and 5% CO2 for 5 minutes. To ensure complete detachment, cells were gently scraped using a rubber cell scraper. After counting with a hemocytometer, cells were seeded in microglia culture medium on a 24-well plate.

Induced pluripotent stem-cell derived microglia-like cells (hiPSC-MGL)

Human induced pluripotent stem cells (iPSC; cell line BIHi250-A, see https://hpscreg.eu/cell-line/BIHi250) were provided by the Berlin Institute of Health (BIH) Core Unit pluripotent Stem Cells and Organoids (CUSCO). hiPSCs were then differentiated into hiPSC-derived microglia-like cells (MGL) using a previously published protocol [17, 21]. In brief, hiPSCs were initially differentiated into hematopoietic progenitor cells over 11 days using a hematopoietic differentiation medium (HDM). From day 0 to day 4 cells were maintained in STEMdiff™ hematopoietic Differentiation Medium A. From day 4 until day 10 STEMdiff™ Heamotpoietic Differnetiation Medium B was applied. On day 10, cells were harvested and FACsorted based on CD43, CD45 and CD 34 expression. CD43+/CD45+ cells were then transferred to microglia differentiation medium (MDM) composed of phenol-free DMEM/F12 (1:1), ITS-G (2% v/v), B27 (2% v/v), N2 (0.5% v/v), monothioglycerol (400 µM), Glutamax (1X), NEAA (1X), and additional insulin (5 µg/ml) for another 28 days. MDM was supplemented as follows: from days 10 to 35 with M-CSF (25 ng/ml), IL-34 (100 ng/ml), and TGFb-1 (50 ng/ml); and from days 35 to 38 with M-CSF (25 ng/ml), IL-34 (100 ng/ml), TGFb-1 (50 ng/ml), CD200 (100 ng/ml), and CX3CL1 (100 ng/ml). After 38 days of differentiation, hiPSC-MGL were harvested and plated for downstream analysis.

For electrophysiological recordings cells were plated on poly-L-lysin for mMG and hMG or vitronectin for hiPSC-MGL coated glass cover slips in a 24-well plate at a density of 10.000 cells/well. For immunological stainings cells were plated in 12-well chamber slides at a density

of 5.000 cells/well. For qPCR, cells were plated in 96-well plates at a density of 20.000 cells/well (mMG), 30.000 cells/well (hMG), or 40.000 cells/well (hiPSC-MGL). Cells were then incubated overnight at 37°C and 5% CO2 to allow for attachment and adaptation before stimulation with either 1 µg/ml LPS, 200 ng/ml IFN-γ, or both for 24 hours.

Patch-clamp recordings

Cover slides with cells were placed in a custom-made patch clamp setup. Bright field images were registered using an upright monocular phototube (Leica, Bensheim, Germany) and a CCD camera (8-bit, Sanyo, Osaka, Japan) at 60X magnification.

Cells were submerged in carbogenated artificial cerebrospinal fluid (aCSF) (129 mM NaCl, 1.25 mM NaH_2PO_4, 1.6 mM $CaCl_2$, 3 mM KCl, 1.8 mM $MgSO_4$, 21 mM $NaHCO_3$ and 10 mM Glucose; adjusted to 300-310 mOsm; all by Carl Roth GmbH, Karlsruhe, Germany) at room temperature. Intracellular solution consisted of 120 mM KCl, 5 mM NaCl, 2 mM $MgCl_2$, 1 mM $CaCl_2$, 10 mM HEPES, 11 mM EGTA (adjusted to pH 7,3 with KOH, 290-300 mOsm). Channel antagonists ML133 (20 µM) and 4-AP (1 mM) were washed in during patch clamp recordings as indicated.

Borosilicate pipettes (Science Products, Hofheim, Germany; 1.5 mm outer diameter) were pulled using a Narishige PC-10 vertical puller (London, UK; electrode resistance of 4-6 MOhm). Pipettes were placed on an Axon Instruments headstage CV-7B (sample rate 100 kHz, low-pass filter 10 kHz (8-pole Bessel Filter)), transmitting the signal to Axon CAN MultiClamp 700B (Axon Instruments, Union City, CA, USA). Signals were digitized through the Axon Digidata 1550 (Axon Instruments). Data was processed with the Multiclamp and pClamp 10 software. Cells were clamped at either -20 mV or -70 mV holding potential (as indicated in the legends). Voltage steps of 50 ms duration were applied from -170 mV to +70 mV with increasing steps of 10 mV.

Isolation of mRNA and qPCR

RNA was extracted from cultured cells using the NucleoSpin® RNA XS kit (Macherey-Nagel, Düren, Germany). For reverse transcription, M-MLV reverse transcriptase and random hexamers were employed to convert RNA into cDNA. Polymerase chain reaction (PCR) amplification was carried out using gene-specific primers and Light Cycler® 480 SYBR Green I Master (Roche Diagnostics, Indianapolis, IN, USA). The PCR conditions were as follows: preincubation at 95°C for 10 minutes, followed by 45 cycles of 95°C for 10 seconds, primer-specific annealing temperature for 10 seconds, and 72°C for 15 seconds. Crossing points of the amplified products were determined using the Second Derivative Maximum Method (Light Cycler Version LCS480 1.5.0.39, Roche). mRNA expression levels were quantified relative to tripeptidyl peptidase 2 (*TPP2*). The specificity of the PCR products was confirmed by melting curve analysis. PCR products were also analyzed on a 1.5% agarose gel to verify the presence of a single amplicon of the expected size. Negative controls, including reactions lacking either template DNA or reverse transcriptase, showed no bands on the gel.

Immunocytochemistry

mMG, hiPSC-MGL, and hMG were fixed for 20 minutes at room temperature using 4% paraformaldehyde (PFA). The cells were then washed three times with 1× tris-buffered saline (TBS). Non-specific binding was blocked with TBS blocking buffer (TBS+), consisting of 1× TBS, 3% normal donkey serum (NDS), and 0.1% Triton X-100 (stock solution: 10%) for 30 minutes. Primary antibodies in TBS+ were incubated overnight at 4°C. Secondary antibody was diluted in 1× TBS and species-specific donkey anti-species serum. After washing with 1x TBS, secondary antibodies were applied at a dilution of 1:400 and incubated for two hours. The cells were then washed again, and Hoechst (1.4 µg/mL), diluted in 1× TBS, was used for nuclear staining.

Confocal microscopy

Microscopy imaging was performed using the confocal laser scanning microscope LSM 700 (Zeiss) equipped with a 40×, 1.3 NA oil objective. Representative images were obtained from random regions of the cultures as *z*-stacks with dimensions of 1,024 × 1,024 pixels in *xy*, 4 *z*-planes, and a pixel size of 0.312 × 0.312 µm.

Image processing and morphological analysis

The morphological analysis was performed using a customized macro script in ImageJ (version 1.54f)[22]. The script applies filters to enhance the signal-to-background ratio and then creates a maximum intensity projection. The automatic thresholding algorithm “Li” was applied, followed by a series of binary operations and size filtering to fill holes and filter out small background objects. Touching cells were automatically separated by applying a watershed based on a seed image created by thresholding a distance map image using functions from the 3D ImageJ Suite plugin [23]. Objects crossing the image borders were automatically excluded. Errors in automatic segmentation were corrected manually by separating unseparated objects, excluding overlapping or merged cells with obscure borders, and manually labeling faint cellular parts that were not detected automatically. Morphological features were then extracted using the MorphoLibJ plugin and the skeleton analysis functions of ImageJ [24]. Statistical analysis was performed on selected representative features, e.g., perimeter-to-area ratio, circularity, maximum calliper diameter.

Statistical analysis

Electrophysiological data were analyzed using custom written Matlab (Version 2021b, MathWorks, Natick, MA, USA) scripts. I/V curves were derived from the last 10 ms of each voltage pulse. Capacitance was derived from I/V curves. Inward current density was calculated at -120 mV to -100 mV and related to the cell capacitance.

Statistical analysis was performed using GraphPad Prism Version 10.2.1 (GraphPad, San Diego, CA, USA). Only for the morphological analysis, statistical testing war performed in Python using Pingouin and scikit-posthocs libraries [25, 26]. Values are represented as box plot with median, interquartile range whiskers from minimum to maximum. For the morphology analysis the whiskers were chosen to indicate 1.5x IQR, as the groups were sufficiently large. Each dot represents one measurement or cell, as indicated in the legends. The different treatment groups were compared using the Kruskal-Wallis test followed by Dunn's test for multiple comparisons, unless indicated otherwise in the legends. Differences were estimated as significant for $p<0.05$ and indicated with an asterisk.

Graphical representation and figures were assorted using CorelDRAW Graphics Suits X7 (Corel Corporation, Ottawa, Canada).

Results

hiPSC-MGL display homeostatic microglia markers and respond to stimulation

mMG, hMG and hiPSC-MGL were cultured and characterized by immunocytochemistry and cytokine transcription to evaluate their microglial identity and validate their suitability for subsequent investigations. mMG were isolated from the brains of postnatal day 3 C57BL/6 mice. hMG were isolated from resected brain tissue obtained from patients undergoing epilepsy surgery. Only tissue from non-pathological regions was used to reflect healthy human microglia. hiPSCs were differentiated into hematopoietic progenitor cells, followed by further differentiation into MGL. All microglia populations, including mMG, hMG, and hiPSC-MGL, were analyzed for the expression of classical microglial markers, the transmembrane protein 119 (TMEM119), C-X3-C motif chemokine receptor 1 (CX3CR1), and protein tyrosine phosphatase receptor type c (CD45). Positive immunostaining for these markers was observed

252 across all microglia groups, confirming their microglial phenotype, as previously shown (Fig.
253 1B, Fig. 3A)[17, 27].

254 To assess microglial reactivity, cells were stimulated for 24 hours with lipopolysaccharide
255 (LPS), interferon-gamma (IFN-γ), or a combination of both (LPS+IFN-γ), a protocol known to
256 induce a robust proinflammatory phenotype in rodent microglia [28]. LPS and IFN-γ signaling
257 pathways converge on the transcription factors nuclear factor kappa B (NFκB) and signal
258 transducer and activator of transcription 1 (STAT1), resulting in an amplified inflammatory
259 response [29]. As stimulation of microglia leads to the transcription of cytokines, we used
260 quantitative real-time PCR (qPCR) to quantify messenger RNA (mRNA) expression levels of
261 the proinflammatory cytokines tumor necrosis factor α (*TNFα*) and interleukin 6 (*IL6*), the
262 transcription factor interferon regulatory factor 1 (*IRF1*), and the chemokine C-X-C motif
263 chemokine ligand 11 (*CXCL11*) [30]. All microglial cell lines exhibited comparable stimulus-
264 dependent proinflammatory responses to LPS and/or IFN-γ, with the strongest responses
265 observed under combined stimulation conditions across all cell types (Fig. S1).

266 The results demonstrate that mMG and hMG retain their distinct microglial identity *in vitro*, as
267 shown by the consistent expression of key microglial markers. Importantly, hiPSC-MGL
268 exhibited robust expression of microglial markers, indicating successful differentiation.
269 Furthermore, all cells expressed proinflammatory cytokines, indicating their responsiveness to
270 the presented stimuli.

271 **Patch-clamp recordings show only few alterations of cell capacity in hMG and hiPSC-**
272 **MGL after stimulation**

273 The functional state of microglia was assessed using single-cell patch-clamp recordings
274 following stimulation with proinflammatory agents. Recordings were performed in voltage
275 clamp and membrane properties were derived from the measured IV-curves (Fig. 2A).

In mMG, stimulation with LPS+IFN-γ resulted in a significant increase in cell capacitance compared to all other groups (Fig. 2B). hMG were the most homogeneous group in terms of cell capacitance (Fig. 2C). hiPSC-MGL exhibited an increase in capacitance following LPS+IFN-γ (Fig. 2D). Overall, hiPSC-MGL displayed lower capacitance than mMG and hMG (note different scale). In summary, mMG demonstrated distinct electrophysiological changes regarding cell capacitance, while the changes of hMG and hiPSC-MGL were less pronounced.

hMG but not mMG increase K_{ir}2.1 currents upon activation with LPS and IFN-γ

Next, we performed a detailed analysis to characterize specific microglial currents, starting with an inward current with time-dependent inactivation. For mMG, this inward current displayed the highest current density under control conditions, with a significant downregulation observed following stimulation with LPS alone and in combination with IFN-γ. Stimulation with IFN-γ did not significantly alter the current density (Fig. 2B). Microglia isolated from adult mice also displayed a reduction in inward current density following stimulation with LPS+IFN-γ (Fig. S2D). Inversely, hMG showed a significant enhancement of the inward current following IFN-γ stimulation, with an even more pronounced increase observed after combined LPS+IFN-γ treatment (Fig. 2C). In hiPSC-MGL, stimulation with LPS and/or IFN-γ did not result in a significant increase in inward current conductivity; however, there was a general trend towards stronger currents following proinflammatory stimulation (Fig. 2D).

The inward current's characteristics of time-dependent inactivation at low voltages suggested the involvement of the inward rectifying potassium channel K_{ir}2.1 (Fig. S2A) [11]. To investigate this, we performed qPCR of mRNA levels of the potassium inwardly rectifying channel subfamily J member 2 (*KCNJ2*), the gene encoding the K_{ir}2.1 channel. In mMG stimulation with LPS and LPS+IFN-γ led to a significant downregulation of *Kcnj2* expression. In hMG a significant increase in *KCNJ2* expression was observed following combined

LPS+IFN-γ stimulation. In hiPSC-MGL LPS and LPS+IFN-γ stimulation resulted in a significant upregulation of *KCNJ2* transcripts (Fig. 2E). These transcriptional alterations mirrored the observed changes in current density, implicating $K_{ir}2.1$ as the most likely ion channel involved. Furthermore, RNA sequencing data from human brain samples published in the Human Protein Atlas and by Olah et al confirm the expression of *KCNJ2* in human microglia (Fig. S2F, G). To prove the role of $K_{ir}2.1$, the specific antagonist ML133 was applied during patch-clamp recordings of mMG exhibiting the characteristic inward current. Indeed, application of ML133 completely abolished the current, supporting the hypothesis that $K_{ir}2.1$ mediates this response (Fig. 2G).

In summary, the $K_{ir}2.1$ channel is downregulated in mMG following stimulation with LPS and LPS+IFN-γ, correlating with a decreased inward current. Conversely, hMG and hiPSC-MGL demonstrate increased expression and functional activity of $K_{ir}2.1$ in response to inflammatory stimuli.

hMG and hiPSC-MGL display no K_v current upon stimulation

The presence of an outward current that was deactivated at a holding potential of -20 mV but could be activated at a holding potential of -70 mV and stimulation above -20 mV, exhibiting delayed activation, was evaluated next (Fig. S2B). This current was detectable in a subset of mMG under control conditions, with a notable increase following stimulation with LPS and/or IFN-γ (Fig. 2F). This current was also present in a small subset of microglia isolated from adult mice (Fig. S2E). The described current characteristics are characteristic of K_v channels. We confirmed this, by applying the K_v channel antagonist 4-AP to mMG exhibiting the delayed-outward current, which led to the current's abolition (Fig. 2H). Remarkably, the K_v current was completely absent in hMG and hiPSC-MGL, both under control conditions and following the various stimulations (Fig. 2F). In line with this, data published in the Human Protein Atlas and the dataset from Olah et al. also failed to show any relevant expression of *KCNA3*, the gene

encoding the prominent K_v channel 1.3, in human microglia under healthy or pathological conditions (Fig. S2F, G).

These findings highlight electrophysiological variability between different species. The absence of K_v currents in hMG and hiPSC-MGL is of particular interest, as it has been discussed as a potential drug target to reduce inflammation in mice.

hMG and hiPSC-MGL do not display amoeboid morphology after stimulation

Microglia are known to alter their morphology as part of their response after exposure to pathological stimuli. Furthermore, ion channel activity and the resting membrane potential are important factors for morphological changes. In order to evaluate cell morphology, we visualized the cells using a CX3CR1-antibody (Fig. 3A) and performed a supervised automated morphological analysis (details see Methods Image Processing and morphological analysis).

In mMG, LPS increased cell circularity, with even greater effects observed under LPS+IFN-γ stimulation. IFN-γ alone increased maximum caliper diameter. All stimuli led to a reduction in the perimeter-to-area ratio, indicating a loss of ramification and shift towards an amoeboid morphology in mMG (Fig. 3B). This reflects the electrophysiological increase in cell capacitance (Fig. 2B). hMG exhibited a more elongated morphology at baseline and only few morphological changes after stimulation. IFN-γ induced a slight decrease in perimeter/area, and LPS+IFN-γ led to a modest increase in caliper diameter, with no major alterations in circularity (Fig. 3C). In hiPSC-MGL, LPS and LPS+IFN-γ decreased circularity and increased caliper diameter, while LPS+IFN-γ also decreased perimeter/area (Fig. 3D). As numbers of end-point voxels were also increased, this indicates a more ramified morphology after stimulation (Fig. S3D).

Overall, mMG displayed a more ameboid morphology following stimulation with LPS+IFN-γ, whereas hMG did not show strong morphological alterations. In contrast, hiPSC-MGL reacted with increased ramification to the stimulation.

Discussion

Microglia express a range of ion channels which are correlated to different functional states and are being evaluated as potential drug targets. However, microglial ion channel activity has mostly been studied in rodent microglia with little information being available from human microglia. Geirsdottir et al. showed that microglia express core genes across species, however notable differences were found in several gene modules between rodent and human microglia, raising the question regarding the translation of mouse data to the human situation [31]. Differences between human and murine microglial sensosome have been described particularly in the context of pathology, constituting a particular translational challenge [32].

Therefore, in this study, we investigated the functional response of human microglia, using hMG and hiPSC-MGL, in established stimulation protocols and compared them with mMG. Our work yielded the following major results: first, we did not see K_v currents in hMG; second, $K_{ir}2.1$ is regulated differently in hMG than in mMG; and third, hiPSC-MGL exhibit similar electrophysiological properties to hMG.

We showed the presence of an outward-rectifying potassium current in mMG which was increased after stimulation, in mMG isolated from both postnatal and adult mice. Notably, this current was absent in hMG and hiPSC-MGL under all stimulation conditions. The outward current's dynamics and sensitivity to 4-AP confirmed its classification within the voltage-gated K_v family. This is consistent with previous evidence identifying these currents as $K_v1.3$ and/or $K_v1.5$ mediated [33, 34]. $K_v1.3$ is of particular interest, as its activity has been linked to

induction of a microglial proinflammatory state [33, 35]. However, $K_v1.3$ studies employing patch-clamp techniques have mainly been performed in animal models or immortalized rodent cell lines such as BV2 [36, 37]. Studies have identified $K_v1.3$ as a potential microglial drug target in various neurological diseases, such as Parkinson's disease, stroke or Alzheimer's disease [14, 38, 39]. While $K_v1.3$ expression has been demonstrated in human T-cells and pulmonary macrophages, electrophysiological evidence for $K_v1.3$ in human microglia remains lacking [40-42]. Reports of detection of $K_v1.3$ in human microglia rely primarily on indirect detection methods (e.g., Western blot, immunocytochemistry, or PCR), leaving a gap in functional data [15, 38, 39]. Furthermore, evidence is inconsistent, as single-cell sequencing and the human protein atlas show little to no microglial *KCNA3* transcription [43]. The data of Olah et al. also indicate no clear upregulation of *KCNA3* in an aged human population or in Alzheimer's disease patients [44, 45]. Our data suggest that the $K_v1.3$ channel may not be active in human microglia. Furthermore, the intact cytokine transcription suggests a K_v-independent activation of a proinflammatory state in hMG. Similarly, Nguyen et al. previously described a lack of K_v current in patch-clamp recordings of cultured human microglia [46]. Interestingly, the comprehensive proteome database of human and mouse microglia of Lloyed et al. shows a lack of $K_v1.3$ in both hMG and human embryonic stem-cell derived (hESC)-MGL, whereas it could be detected in xenografted-hESC-MGL to mice, suggesting a context-dependent expression in human microglia [47]. The discrepancy in $K_v1.3$ activity in human and mouse microglia could partly explain the translational failure of $K_v1.3$-targeting microglial therapies and highlights the need to carefully consider species- and context-dependent channel expression.

Consistent with prior reports in rodent microglia, we found that mMG exhibited a prominent inward-rectifying potassium current ($K_{ir}2.1$) at baseline [9, 11]. Interestingly, this current is typically absent in rodent microglia *in vivo* unless exposed to pathogenic stimuli, suggesting

that *in vitro* isolation procedures may inadvertently induce a pre-activated state in mMG [9]. Contrary to *in vivo*, $K_{ir}2.1$ current density decreased in mMG from both postnatal and adult mice following LPS+IFN-γ stimulation. This goes in line with the depolarized reversal potential, as $K_{ir}2.1$ contributes to stabilizing the resting membrane potential. In hMG, however, stimulation led to an increase in $K_{ir}2.1$ currents, resembling the activation profile observed in mouse microglia *in vivo* [4]. This high expression of $K_{ir}2.1$ can be correlated to the retained elongated microglial morphology of hMG, even after stimulation. This correlation was even stronger in hiPSC-MGL. The membrane potential determines the driving force for calcium entry, linking hyperpolarization to rapid stimulus–response coupling and a more ramified microglial morphology [34, 48]. In the dataset published by Olah et al the expression of *KCNJ2* is mainly upregulated in clusters associated with an anti-inflammatory profile (Fig. S2G) [44]. Meanwhile, the antagonism of $K_{ir}2.1$ has also been shown to reduce proliferation and migration in rodent microglia [11, 49]. These findings suggest different regulatory mechanisms of $K_{ir}2.1$ in human and mouse microglial responses to proinflammatory signals *in vitro*. Furthermore, the lack of amoeboid morphology following stimulation of human microglia correlates with $K_{ir}2.1$ activity. Further studies are necessary to better understand the specific mechanistic function of $K_{ir}2.1$ in morphology and inflammatory response.

We demonstrated that hiPSC-MGL exhibited robust expression of microglial markers, indicating successful differentiation, comparable to primary microglia. These findings validate the use of hiPSC-MGL as a reliable model for further mechanistic studies, as previously shown [6, 17]. We also showed that hiPSC-MGL were responsive to the stimulation with LPS and/or IFN-γ, as it led to an increase in transcription of proinflammatory cytokines, which was largely consistent across cell types and in line with existing literature [18, 50, 51]. We could show that single-cell patch-clamp recordings were not just feasible but also hold a lot of potential for hiPSC-MGL. Furthermore, they more closely mirrored hMG reactivity to inflammatory stimuli

than mMG, exhibiting no K_v currents while showing a tendency toward increased $K_{ir}2.1$ activity upon stimulation. Interestingly, they showed an increased ramification after stimulation. Overall, these changes go in line with the described alterations in hMG, and in opposition to mMG. Functional studies on hMG remain rare due to limited tissue availability and technical challenges in *in situ* labeling, further underscoring the value of hiPSC-MGL [52]. The use of hMG and hiPSC-MGL allowed for a significant reduction in animals needed for this study. Although animal-derived supplements were still used in this study, the models offer the possibility of working completely animal-free, such as by using recombinant proteins from HEK cells [53, 54]. This reduces the reliance on animal experiments and the ethical concerns associated with animal use.

In summary, our study underscores critical differences between mouse and human microglia in terms of electrophysiological properties, ion channel expression as a potential drug target, and morphology. Although mMG remain a widely used model system, our data highlight important species-specific differences that might explain translational inconsistencies. The use of hiPSC-MGL is a promising bridging technology and reduces animal numbers in scientific experiments. Incorporating human-derived microglia into preclinical pipelines may therefore help bridge the translational gap between experimental findings and clinical outcomes.

Limitations of the study

A possible limitation of this study is the varied cell age, as microglial phenotype and receptor expression are known to vary across developmental stages and with aging [55]. mMG were isolated at postnatal day 3 as this constitutes a well-established reference system, widely used in numerous studies and forming the basis for further investigations, particularly in pathological contexts. Culturing adult mouse microglia entails several known technical limitations, including low yield and purity, and reduced viability [56, 57]. However, we could show similar ion current patterns in postnatal and adult mouse microglia. Furthermore, it is

known that microglia from adult rodents show strong K_v and $K_{ir}2.1$ currents following pathological stimulation *in vivo* [4, 9]. The hiPSC-MGLs originated from reprogrammed fibroblasts of adult donors, and hMG were isolated from adult surgical specimens. This heterogeneity in donor age may contribute to differences in microglial responses; however, the most pronounced effects regarding potassium current presence were observed between murine and human cells, regardless of age.

Additionally, differences in culture conditions could have influenced cellular behavior. The medium used for hiPSC-MGLs contained macrophage colony-stimulating factor (M-CSF), which is known to enhance microglial proliferation and phagocytic activity [58]. IL-34, also contained in the MGL culture medium, has been associated with the promotion of a more mature and neuroprotective microglial phenotype [59]. In contrast, mMG and hMG were not exposed to M-CSF or IL-34. Both mMG and hMG incubation media included fetal calf serum, however, which has previously been reported to induce microglial phagocytic activity [60, 61]. While these supplements are standard in microglial differentiation protocols, they may also contribute to variability in functional response to stimuli.

Resource Availability

Lead contact

Requests for further information and resources should be directed to and will be fulfilled by the corresponding author, Karen Gertz (karen.gertz@charite.de).

Material availability

This study did not generate new unique reagents.

Data and code availability

All data reported in this paper will be shared by the lead contact upon request.

This paper does not report original code.

Any additional information requires to reanalyze the data reported in this paper is available from the lead contact upon request.

Acknowledgment

The authors would like to acknowledge the support of the Berlin Institute of Health Core Unit pluripotent Stem Cells and Organoids (CUSCO) for providing the hiPSC line. This study was supported by the Deutsche Forschungsgemeinschaft (Priority Program 2395/GE, 2576/6-1 to K.G.; Germany´s Excellence Strategy—EXC-2049—390688087 to M.E.; Collaborative Research Center ReTune TRR 295- 424778381 to M.E.; Clinical Research Group KFO 5023 BeCAUSE-Y, project 2 EN343/16-1 to M.E.), the Bundesministerium für Bildung und Forschung (CSB to M.E., and K.G.), the German Center for Neurodegenerative Diseases (DZNE to M.E.), the German Center for Cardiovascular Research (DZHK to M.E. and K.G.), the German Center for Mental Health (DZPG to M.E.). We would like to thank Jan-Oliver Hollnagel in particular for his support in creating the MATLAB script for analyzing the electrophysiological data. Special thanks go to Melanie Kroh, Stefanie Balz and Bettina Herrmann for their excellent technical assistance.

Author contribution

S.S., R.G., and K.G. conceived this study. S.S. performed the electrophysiological experiments. J.F. and R.G. performed cell culturing, immunostaining and microscopy. S.S. analyzed the data and M.K. performed the morphological analysis. A.P. and J.H. collected human brain tissue. J.O., T.S., T.K., M.S. performed neurosurgical procedures. S.S., R.G. and

493 K.G. wrote the manuscript with input from all authors. All authors discussed the results and
494 commented on the final manuscript.

495 Declaration of interests

496 The authors declare no competing interests.

497

498 Figures

499

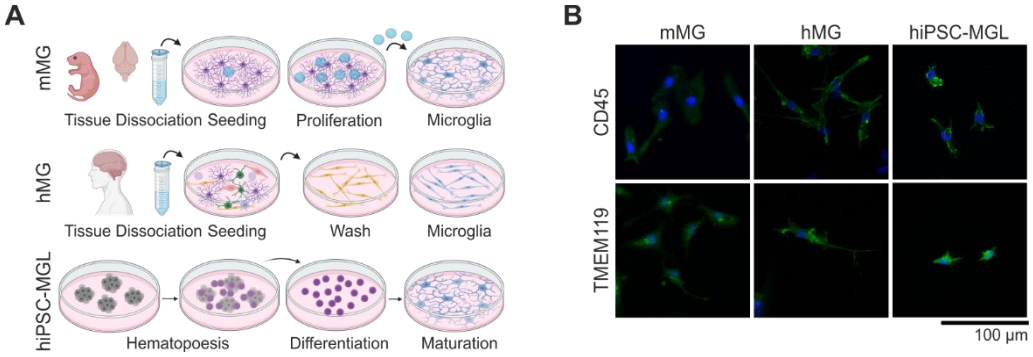

500

501 **Figure 1: mMG, hMG and hiPSC-MGL express microglial markers**

502 **(A)** Schematic of different sources of primary mouse microglia (mMG), primary human
503 microglia (hMG), and human induced pluripotent stem cell-derived microglia-like cells
504 (hiPSC-MGL). Created in BioRender. Göttert, R (2025) **(B)** Maximum intensity projections of
505 confocal laser scanning microscopy images for mMG, hMG, and hiPSC-MGL, labeled for
506 microglial maturations markers CD45 or TMEM119 (green) and Hoechst (blue). Scale bar 100
507 µm.

508

509

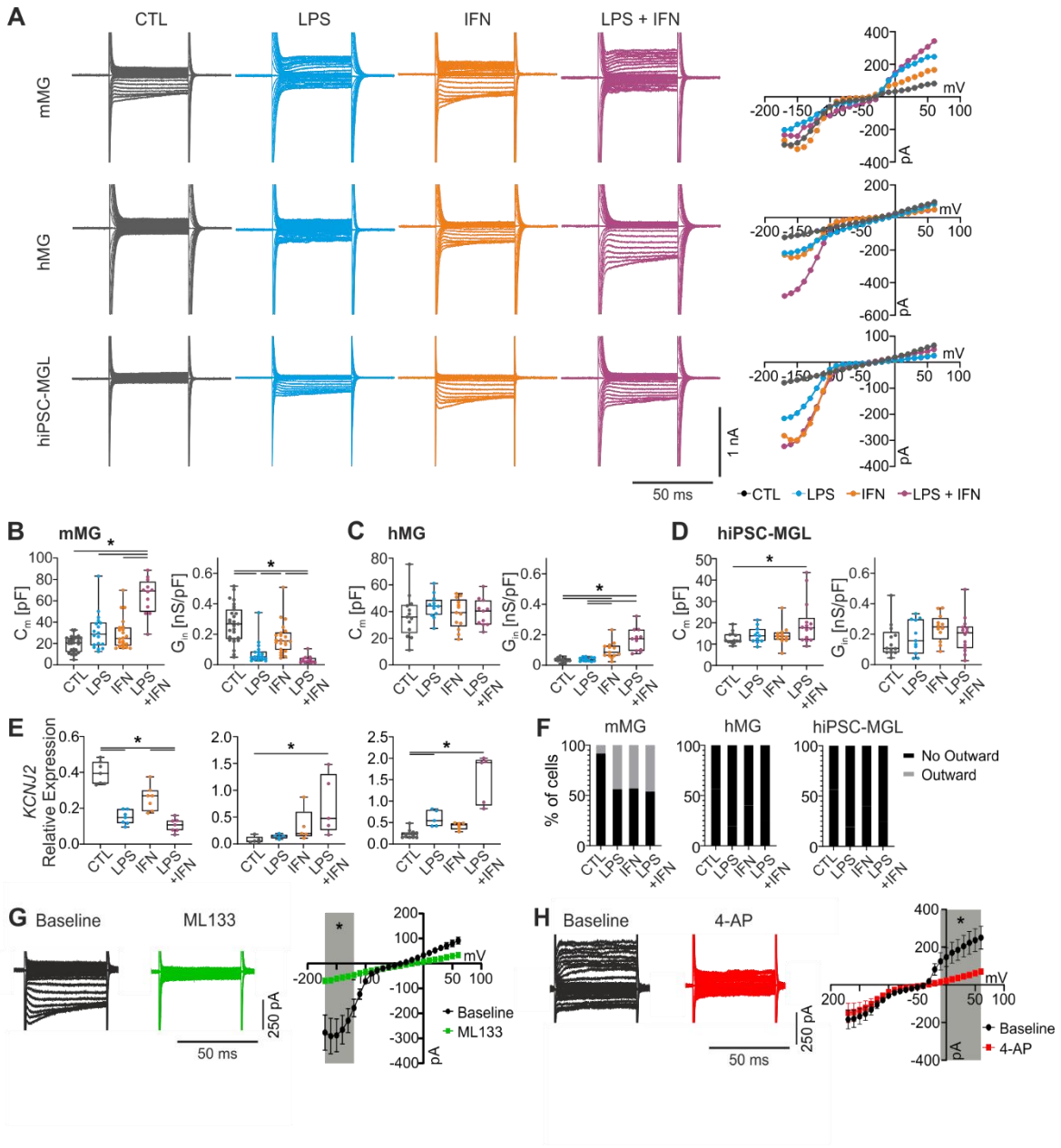

Figure 2: $K_{ir}2.1$ is differently regulated in hMG and hiPSC-MGL than mMG, with no detection of K_v current in hMG or hiPSC-MGL.

(A) Single-cell patch-clamp recordings of microglial cells were performed following the indicated stimulation. Representative traces of recordings at a holding potential of -70 mV of mMG, hMG, and hiPSC-MGL are shown with their corresponding IV-curves. **(B-D)** Membrane capacitance (C_m) and inward current density (G_{in}) was derived from IV-curve of whole cell patch clamp recordings at a holding potential of -20 mV. Please note the different

scaling for capacitance. Statistical analysis with Kruskal-Wallis test followed by Dunn's test for multiple comparisons, $*P < 0.05$. Data represented as box plots with median, each dot represents one cell. For n=recordings: mMG (CTL=14, LPS=10, IFN=12, LPS+IFN=12), iPSC-MGL (CTL=13, LPS=12, IFN=12, LPS+IFN=10), hMG (CTL=11, LPS=11, IFN=12, LPS+IFN=11) **(E)** mRNA expression of *KCNJ2* was quantified by qPCR and is represented relative to householding gene *TPP2*. For n=samples: mMG (CTL=7, LPS=7, IFN=7, LPS+IFN=7), iPSC-MGL (CTL=12, LPS=5, IFN=6, LPS+IFN=5), hMG (CTL=5, LPS=5, IFN=5, LPS+IFN=5) **(F)** Percentage of cells exhibiting voltage-dependent, delayed outward current at a holding potential of -70 mV and activation at stimulation of -20 mV. N as for D-F. **(G)** Patch clamp recordings were performed before (black) and after (green) wash-in of specific $K_{ir}2.1$ antagonist ML133 (holding potential -20 mV) in primary mouse microglia. **(H)** Patch clamp recordings were performed before (black) and after (green) wash-in of K_v antagonist 4-AP (holding potential -70 mV) in primary mouse microglia. IV-curves are represented as mean and standard error of the mean. Statistical analysis with two-way ANOVA and Sidak's test for multiple comparisons, grey area indicates $*P < 0.05$. Statistical analysis with Wilcoxon test, $*P < 0.05$. n=8.

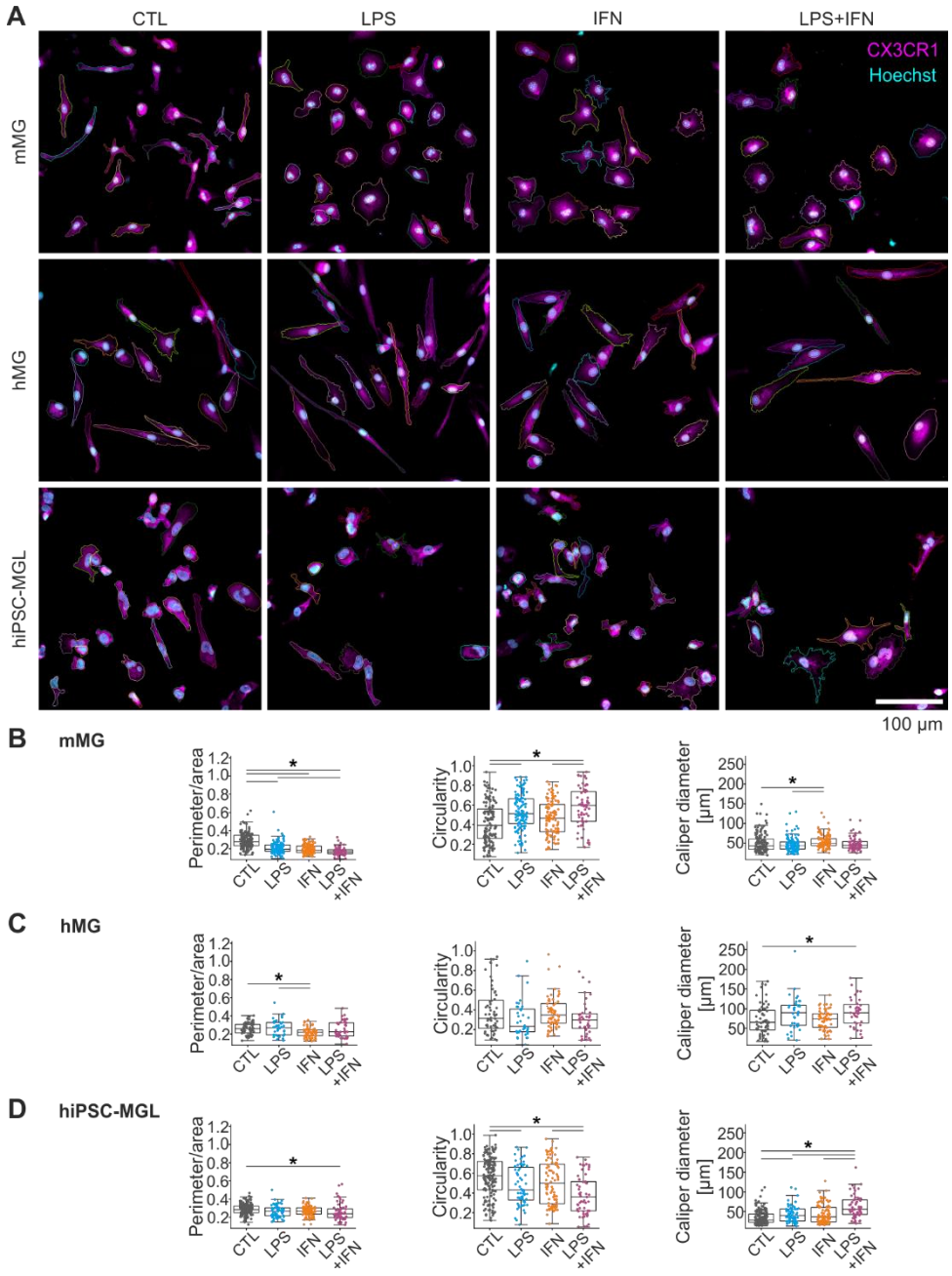

Figure 3: hMG show little morphological alterations, while hiPSC-MGL increase ramification after stimulation

(A) Maximum intensity projections of confocal laser scanning microscopy images for cultured cells from the studied cell lines under four treatment conditions, labeled with CX3CR1-AF488 (magenta) and Hoechst (cyan). The colored borders of cells and nuclei represent the segmentation results of the morphological analysis. Cells were excluded if they crossed the image borders, overlapped with other cells, or merged with other cells with obscure borders.

Scale bar 100 µm. **(B-D)** Statistical analysis of several morphological features quantifying the morphological changes of cultured cells under the treatment conditions. Statistical analysis with Kruskal-Wallis test followed by Dunn's test for multiple comparisons, $*P < 0.05$. Data represented as box plot with median. Each dot represents one cell.

For n=cells: mMG (CTL=135, LPS=123, IFN=107, LPS+IFN=63), iPSC-MGL (CTL=154, LPS=63, IFN=88, LPS+IFN=57), hMG (CTL=60, LPS=38, IFN=61, LPS+IFN=39).

552 **References**

553 1. Li, Q. and B.A. Barres, *Microglia and macrophages in brain homeostasis and*
554 *disease.* Nat Rev Immunol, 2018. **18**(4): p. 225-242.

555 2. Schilling, S., et al., *TLR2- and TLR3-activated microglia induce different levels of*
556 *neuronal network dysfunction in a context-dependent manner.* Brain Behav Immun,
557 2021. **96**: p. 80-91.

558 3. Kettenmann, H., et al., *Physiology of microglia.* Physiol Rev, 2011. **91**(2): p. 461-553.

559 4. Kikhia, M., et al., *Multicolor fate mapping of microglia reveals polyclonal*
560 *proliferation, heterogeneity, and cell-cell interactions after ischemic stroke in mice.*
561 Nature Communications, 2025. **16**(1): p. 8294.

562 5. Hanisch, U.K., *Microglia as a source and target of cytokines.* Glia, 2002. **40**(2): p.
563 140-155.

564 6. Haenseler, W., et al., *A Highly Efficient Human Pluripotent Stem Cell Microglia*
565 *Model Displays a Neuronal-Co-culture-Specific Expression Profile and Inflammatory*
566 *Response.* Stem Cell Reports, 2017. **8**(6): p. 1727-1742.

567 7. Izquierdo, P., D. Attwell, and C. Madry, *Ion Channels and Receptors as Determinants*
568 *of Microglial Function.* Trends in Neurosciences, 2019. **42**(4): p. 278-292.

569 8. Kronenberg, G., et al., *Distinguishing features of microglia- and monocyte-derived*
570 *macrophages after stroke.* Acta Neuropathologica, 2018. **135**(4): p. 551-568.

571 9. Boucsein, C., H. Kettenmann, and C. Nolte, *Electrophysiological properties of*
572 *microglial cells in normal and pathologic rat brain slices.* European Journal of
573 Neuroscience, 2000. **12**(6): p. 2049-2058.

574 10. Seifert, S., et al., *Transmitter- and hormone-activated Ca(2+) responses in adult*
575 *microglia/brain macrophages in situ recorded after viral transduction of a*
576 *recombinant Ca(2+) sensor.* Cell Calcium, 2011. **49**(6): p. 365-75.

577 11. Lam, D. and L.C. Schlichter, *Expression and contributions of the Kir2.1 inward-*
578 *rectifier K+ channel to proliferation, migration and chemotaxis of microglia in*
579 *unstimulated and anti-inflammatory states.* Frontiers in Cellular Neuroscience, 2015.
580 **9**(185).

581 12. Di Lucente, J., et al., *The voltage-gated potassium channel Kv1.3 is required for*
582 *microglial pro-inflammatory activation in vivo.* Glia, 2018. **66**(9): p. 1881-1895.

13. Fomina, A.F., H.M. Nguyen, and H. Wulff, *Kv1.3 inhibition attenuates neuroinflammation through disruption of microglial calcium signaling.* Channels, 2021. **15**(1): p. 67-78.

14. Chen, Y.-J., et al., *Inhibition of the potassium channel Kv1.3 reduces infarction and inflammation in ischemic stroke.* Annals of Clinical and Translational Neurology, 2018. **5**(2): p. 147-161.

15. Maezawa, I., et al., *Kv1.3 inhibition as a potential microglia-targeted therapy for Alzheimer's disease: preclinical proof of concept.* Brain, 2018. **141**(2): p. 596-612.

16. Rangaraju, S., et al., *Potassium Channel Kv1.3 Is Highly Expressed by Microglia in Human Alzheimer's Disease.* Journal of Alzheimer's Disease, 2015. **44**(3): p. 797-808.

17. Göttert, R., et al., *Lithium inhibits tryptophan catabolism via the inflammation-induced kynurenine pathway in human microglia.* Glia, 2022. **70**(3): p. 558-571.

18. Abud, E.M., et al., *iPSC-Derived Human Microglia-like Cells to Study Neurological Diseases.* Neuron, 2017. **94**(2): p. 278-293.e9.

19. Hellmann-Regen, J., et al., *Accelerated degradation of retinoic acid by activated microglia.* J Neuroimmunol, 2013. **256**(1-2): p. 1-6.

20. Rustenhoven, J., et al., *Isolation of highly enriched primary human microglia for functional studies.* Scientific Reports, 2016. **6**(1): p. 19371.

21. Mcquade, A. and M. Blurton-Jones, *Human Induced Pluripotent Stem Cell-Derived Microglia (hiPSC-Microglia)*, in *Methods in Molecular Biology*. 2021, Springer US. p. 473-482.

22. Schindelin, J., et al., *Fiji: an open-source platform for biological-image analysis.* Nat Methods, 2012. **9**(7): p. 676-82.

23. Ollion, J., et al., *TANGO: a generic tool for high-throughput 3D image analysis for studying nuclear organization.* Bioinformatics, 2013. **29**(14): p. 1840-1841.

24. Legland, D., I. Arganda-Carreras, and P. Andrey, *MorphoLibJ: integrated library and plugins for mathematical morphology with ImageJ.* Bioinformatics, 2016. **32**(22): p. 3532-3534.

25. Vallat, R., *Pingouin: statistics in Python.* Journal of Open Source Software, 2018. **3**(31): p. 1026.

26. Terpilowski, M., *scikit-posthocs: Pairwise multiple comparison tests in Python.* Journal of Open Source Software, 2019. **4**(36): p. 1169.

615 27. Uhlemann, R., et al., *Actin dynamics shape microglia effector functions.* Brain Struct
616 Funct, 2016. **221**(5): p. 2717-34.

617 28. Papageorgiou, I.E., et al., *TLR4-activated microglia require IFN-γ to induce severe*
618 *neuronal dysfunction and death in situ.* Proceedings of the National Academy of
619 Sciences, 2016. **113**(1): p. 212-217.

620 29. Schroder, K., M.J. Sweet, and D.A. Hume, *Signal integration between IFNgamma*
621 *and TLR signalling pathways in macrophages.* Immunobiology, 2006. **211**(6-8): p.
622 511-24.

623 30. Smith, J.A., et al., *Role of pro-inflammatory cytokines released from microglia in*
624 *neurodegenerative diseases.* Brain Res Bull, 2012. **87**(1): p. 10-20.

625 31. Geirsdottir, L., et al., *Cross-Species Single-Cell Analysis Reveals Divergence of the*
626 *Primate Microglia Program.* Cell, 2019. **179**(7): p. 1609-1622.e16.

627 32. Abels, E.R., et al., *Comparative Analysis Identifies Similarities between the Human*
628 *and Murine Microglial Sensomes.* International Journal of Molecular Sciences, 2021.
629 **22**(3): p. 1495.

630 33. Nguyen, H.M., et al., *Differential Kv1.3, KCa3.1, and Kir2.1 expression in*
631 *"classically" and "alternatively" activated microglia.* Glia, 2017. **65**(1): p. 106-121.

632 34. Lam, D., S. Lively, and L.C. Schlichter, *Responses of rat and mouse primary*
633 *microglia to pro- and anti-inflammatory stimuli: molecular profiles, K+ channels and*
634 *migration.* Journal of Neuroinflammation, 2017. **14**(1).

635 35. Li, B., et al., *Pharmacological inhibition of Kv1.3 channel reduces sevoflurane-*
636 *induced cognitive impairment through NLRP3-dependent microglial modulation.*
637 Brain Res Bull, 2025. **225**: p. 111351.

638 36. Anton, R., et al., *Potassium Channels Kv1.3 and Kir2.1 But Not Kv1.5 Contribute to*
639 *BV2 Cell Line and Primary Microglial Migration.* International Journal of Molecular
640 Sciences, 2021. **22**(4): p. 2081.

641 37. Chen, Y.-J., et al., *The potassium channel KCa3.1 constitutes a pharmacological*
642 *target for neuroinflammation associated with ischemia/reperfusion stroke.* Journal of
643 Cerebral Blood Flow & Metabolism, 2016. **36**(12): p. 2146-2161.

644 38. Sarkar, S., et al., *Kv1.3 modulates neuroinflammation and neurodegeneration in*
645 *Parkinson's disease.* J Clin Invest, 2020. **130**(8): p. 4195-4212.

646 39. Ramesha, S., et al., *Unique molecular characteristics and microglial origin of Kv1.3*
647 *channel–positive brain myeloid cells in Alzheimer's disease.* Proceedings of the
648 National Academy of Sciences, 2021. **118**(11): p. e2013545118.

40. Selvakumar, P., et al., *Structures of the T cell potassium channel Kv1.3 with immunoglobulin modulators.* Nature Communications, 2022. **13**(1).

41. Mackenzie, A.B., H. Chirakkal, and R.A. North, *Kv1.3 potassium channels in human alveolar macrophages.* Am J Physiol Lung Cell Mol Physiol, 2003. **285**(4): p. L862-8.

42. Rus, H., et al., *The voltage-gated potassium channel Kv1.3 is highly expressed on inflammatory infiltrates in multiple sclerosis brain.* Proceedings of the National Academy of Sciences, 2005. **102**(31): p. 11094-11099.

43. Karlsson, M., et al., *A single–cell type transcriptomics map of human tissues.* Science Advances, 2021. **7**(31): p. eabh2169.

44. Olah, M., et al., *Single cell RNA sequencing of human microglia uncovers a subset associated with Alzheimer's disease.* Nature Communications, 2020. **11**(1).

45. Olah, M., et al., *A transcriptomic atlas of aged human microglia.* Nature Communications, 2018. **9**(1).

46. Nguyen, H.M., et al., *Potassium channel expression and function in microglia: Plasticity and possible species variations.* Channels, 2017. **11**(4): p. 305-315.

47. Lloyd, A.F., et al., *Deep proteomic analysis of microglia reveals fundamental biological differences between model systems.* Cell Reports, 2024. **43**(11): p. 114908.

48. Laprell, L., et al., *The role of microglia membrane potential in chemotaxis.* Journal of Neuroinflammation, 2021. **18**(1).

49. Gattlen, C., et al., *The inhibition of Kir2.1 potassium channels depolarizes spinal microglial cells, reduces their proliferation, and attenuates neuropathic pain.* Glia, 2020. **68**(10): p. 2119-2135.

50. Yang, X., V. Diaz, and H. Huang, *The Role of Interferon Regulatory Factor 1 in Regulating Microglial Activation and Retinal Inflammation.* International Journal of Molecular Sciences, 2022. **23**(23): p. 14664.

51. Bsibsi, M., et al., *Demyelination during multiple sclerosis is associated with combined activation of microglia/macrophages by IFN-γ and alpha B-crystallin.* Acta Neuropathologica, 2014. **128**(2): p. 215-229.

52. Palomba, N.P., et al., *ATP-evoked intracellular Ca(2+) transients shape the ionic permeability of human microglia from epileptic temporal cortex.* J Neuroinflammation, 2021. **18**(1): p. 44.

53. Liste-Calleja, L., M. Lecina, and J.J. Cairó, *HEK293 cell culture media study towards bioprocess optimization: Animal derived component free and animal derived component containing platforms.* J Biosci Bioeng, 2014. **117**(4): p. 471-7.

54. Bramwell, L.R., et al., *An Evaluation of the Replacement of Animal-derived Biomaterials in Human Primary Cell Culture.* Alternatives to Laboratory Animals, 2024. **52**(5): p. 247-260.

55. Harry, G.J., *Microglia during development and aging.* Pharmacology & Therapeutics, 2013. **139**(3): p. 313-326.

56. Ngwa, C., et al., *Age and sex differences in primary microglia culture: A comparative study.* Journal of Neuroscience Methods, 2021. **364**: p. 109359.

57. Mizrachi, M. and B. Diamond, *Impact of microglia isolation and culture methodology on transcriptional profile and function.* Journal of Neuroinflammation, 2024. **21**(1).

58. Smith, A.M., et al., *M-CSF increases proliferation and phagocytosis while modulating receptor and transcription factor expression in adult human microglia.* Journal of Neuroinflammation, 2013. **10**(1): p. 85.

59. Devlin, B.A., et al., *Neuron Derived Cytokine Interleukin-34 Controls Developmental Microglia Function*. 2024, Cold Spring Harbor Laboratory.

60. Patrizio, M., et al., *Selective enhancement by serum factors of cyclic AMP accumulation in rat microglial cultures.* Neurochem Int, 1996. **29**(1): p. 89-96.

61. Bohlen, C.J., et al., *Diverse Requirements for Microglial Survival, Specification, and Function Revealed by Defined-Medium Cultures.* Neuron, 2017. **94**(4): p. 759-773.e8.

704 **Resource Table**

705

706 **Table 1: Agents**

REAGENT or RESOURCE	SOURCE	IDENTIFIER
Antibodies		
Anti-CD45 (1:100)	Abd Serotec, Neuried, Germany	Cat # MCA1031GA RRID: AB_324339
Anti-CD45 (human, 1:100)	EXBIO, Praha, Czech Republic	Cat # 11-222-C025 RRID: AB_10732878
Anti-CX3CR1 (human, 1:50)	Bio-Rad, Feldkirchen, Germany	Cat # AHP1589 RRID: AB_2087421
Anti-TMEM119 (1:100)	ATLAS AK, Bromma, Sweden	Cat # HPA051870 RRID: AB_2681645
Anti-mouse (Alexa 488, 1:400)	Invitrogen, Waltham, MA, USA	Cat # A21202 RRID: AB_141607
Anti-rat (Alexa 488, 1:400)	Invitrogen, Waltham, MA, USA	Cat # A21208 RRID: AB_2535794
Anti-rabbit (Alexa 488, 1:400)	Invitrogen, Waltham, MA, USA	Cat # A21206 RRID: AB_2535792
PE anti-human CD45 Antibody (1:20)	BioLegend, San Diego, CA, USA	Cat # 304007 RRID: AB_314395
APC anti-human CD43 Antibody (1:20)	BioLegend, San Diego, CA, USA	Cat # 343205 RRID: AB_2194073
FITC anti-human CD34 Antibody	BioLegend, San Diego, CA, USA	Cat # 343603 RRID: AB_1732030
Bacterial and virus strains		
None		
Biological samples		
None		
Chemicals, peptides, and recombinant proteins		
4-AP	Sigma-Aldrich, St. Louis, MO, USA	Cat # 275875-5G
ML133	Sigma-Aldrich, St. Louis, MO, USA	Cat # SML0190-5MG
LPS from E. coli 055:B5	Sigma-Aldrich, St. Louis, MO, USA	Cat # L4524-10MG
Human IFN-g	Peprotech, Cranbury, NJ, USA	Cat # 300-02
Murine IFN-g	Peprotech, Cranbury, NJ, USA	Cat # 315-05
DMEM	Thermo Fisher, Waltham, MA, USA	Cat # 31966-021
FCS	PAN Biotech Aidenbach, Germany	Cat # P30-3031

Pen/Strep	PAN Biotech, Aidenbach, Germany	Cat # P06-07100
Sodium pyrucate	PAN Biotech Aidenbach, Germany	Cat # P04-43100
D-Glucose	Sigma-Aldrich, St. Louis, MO, USA	Cat # G8769-100ML
STEMdiff	Stemcell Technologies, Vancouver, Canada	Cat # 05311
DMEM/F12	Thermo Fisher, Waltham, MA, USA	Cat # 11039-021
ITS-G	Thermo Fisher, Waltham, MA, USA	Cat # 41400-045
B27	Thermo Fisher, Waltham, MA, USA	Cat # 17504-044
N-2	Thermo Fisher, Waltham, MA, USA	Cat # 17502-048
Monothioglycerol	Sigma-Aldrich, St. Louis, MO, USA	Cat # M1753-100ML
Glutamax	Thermo Fisher, Waltham, MA, USA	Cat # 35050-061
NEAA	Thermo Fisher, Waltham, MA, USA	Cat # 11140-050
Insulin	PAN Biotech, Aidenbach, Germany	Cat # P07-04300
M-CSF	Peprotech, Cranbury, NJ, USA	Cat # 300-25
IL-34	Peprotech, Cranbury, NJ, USA	Cat # 200-34
TGFb1	Peprotech, Cranbury, NJ, USA	Cat # 100-21
CD200	Novoprotein, Shanghai, China	Cat # C311
CX3CL1	Peprotech, Cranbury, NJ, USA	Cat # 300-31-50UG
PBS (no Mg, No Ca)	Thermo Fisher, Waltham, MA, USA	Cat # 14200-067
Trypsin/EDTA	PAN Biotech, Aidenbach, Germany	Cat # P10-024100
PLL	Sigma-Aldrich, St. Louis, MO, USA	Cat # P4707
Vitronectin	Thermo Fisher, Waltham, MA, USA	Cat # A14700

Matrigel	Corning Incorporated, Corning, NY, USA	Cat # 354277
M-MLV reverse transcriptase	Promega, Madison, WI, Germany	Cat # M1701
Random hexamers	Promega, Madison, WI, Germany	Cat # C1181
Agarose gel	Carl Roth GmbH, Karlsruhe, Germany	Cat # 2267.4
Paraformaldehyd	Carl Roth GmbH, Karlsruhe, Germany	Cat # 0335.2
Donkey Serum	Dominique Dutscher, Bernolsheim, France	Cat # S2170-100
Triton X-100	Sigma-Aldrich, St. Louis, MO, USA	Cat # X100-100ML
Hoechst	Abcam, Cambridge, UK	Cat # 33342
Critical commercial assays		
Nucleo Spin RNA kit	Macherev-Nagel, Düren, Germany	Cat # 740902.50
Deposited data		
None		
Experimental models: Cell lines		
BIHi250-A	BIH, Berlin, Germany	https://hpscreg.eu/cell-line/BIHi250-A
Experimental models: Organisms/strains		
C57BL/6J wildtype mice		
Oligonucleotides		
None		
Recombinant DNA		
None		
Software and algorithms		
pClamp 10	Molecular Devices, San Jose, CA, USA	
Matlab (Version 2021b,)	MathWorks, Natick, MA, USA	
GraphPad Prism Version 10.2.1	GraphPad, San Diego, CA, USA	
CorelDRAW Graphics Suits X7	Corel Corporation, Ottawa, Canada	
Other		
Cell scraper	SPL Life Sciences, Pocheon-si, South Korea	Cat # 90021

T75 flask	Corning Incorporated, Corning, NY, USA	Cat # 353136
Glass cover slips, 5 mm	Assistant, Glaswarenfabrik Karl Hecht, Sondheim vor der Rhön, Germany	Cat # 41001
12 well chamber slides	Ibidi, Gräfeling, Germany	Cat # 81201

707

708

709 **Table 2: Primer sequences**

Gene	Forward Primer	Reverse Primer
Tpp2 mouse	CTT CTA TCC AAA GGC TCT CAA GG	CTC TCC AGG TCT CAC CAT CAT G
Kcnj2 mouse	CAA TGG CTT TGG GAA TGG CAA G	GAA GAT AAC CAG CAT CCA CCT C
Tnfa Mouse	CAT CTT CTC AAA ATT CGA GTG ACA A	TGG GAG TAG ACA AGG TAC AAC CC
Il6 Mouse	GAG GAT ACC ACT CCC AAC AGA CC	AAG TGC ATC ATC GTT GTT CAT ACA
Irf1 mouse	CAT TCA CAC AGG CCG ATA CAA AG	CCT TGT TCC TAC TCT GAT CCT TC
Cxcl11 mouse	GCT GCT CAA GGC TTC CTT ATG	CAA CTT TGT CGC AGC CGT TAC
TPP2 human	CAA GCT GGA CAA ATC CCT CAG	CAT CAT GCC ATA CCA AGC AGT C
KCNJ2 human	CTA CAG CAT CGT CTC TTC AGA AG	CAG GCA GAA GAT AAC CAG CAT C
TNFα human	CAG GCA GTC AGA TCA TCT TCT CG	CTG GTT ATC TCT CAG CTC CAC G
IL6 human	CAA ATT CGG TAC ATC CTC GAC G	CAG GCA AGT CTC CTC ATT GAA TC

IRF1 human	CAT TCA CAC AGG CCG ATA CAA AG	GTT CTT GGT GAG AGG TGG AAG C
CXCL11 human	GTT GTT CAA GGC TTC CCC ATG	GTC ACA GTT GTT ACT TGG GTA C

710